Clays and Clay Minerals, Vol. 57, No. 5, 521–530, 2009.

ORIGIN AND MINERALOGY OF SEPIOLITE AND PALYGORSKITE FROM THE TULUANSHAN FORMATION, EASTERN TAIWAN

MING KUANG WANG[1,*], PAO CHUNG TSENG[2], SHYUN SHENG CHANG[2], DAH TONG RAY[2], YEN HONG SHAU[3], YUN WEI SHEN[2], RUEY CHYONG CHEN[4,†], AND PO NENG CHIANG[1]

[1] Department of Agricultural Chemistry, National Taiwan University, Taipei, Taiwan, 10617
[2] Department of Resources Engineering, National Cheng-Kung University, Tainan, Taiwan 70101
[3] Department of Marine Biotechnology and Resources, National Sun Yat-Sen University, Kaoshiung 80424, Taiwan 80424
[4] Department of Geosciences, National Taiwan University, Taipei, Taiwan, 10617

Abstract—The Tuluanshan Formation of the eastern Coastal Range of Taiwan overlies an andesitic core complex presumed to be the source of hydrothermal fluids responsible for the Si- and Mg-rich mineralization of sepiolite and palygorskite (attapulgite) which are found in veins within fissures and in fracture zones of the volcanic rocks of the region. This study was undertaken in order to understand these relationships better by characterizing sepiolite and palygorskite in this Formation and by examining their occurrence and distribution in the Tungho (TH) and Chunjih (CJ) areas. Samples were analyzed using X-ray diffraction (XRD), thermal analysis, Fourier-transform infrared (FTIR) spectroscopy, and petrographic, scanning (SEM), and transmission (TEM) electron microscopic methods. Sepiolite and palygorskite are blocky and earthy-type materials that display fibrous characteristics when viewed using TEM and SEM and occurred alone or with chalcedony in veins. The fibers of blocky sepiolite are commonly intercalated with smectite but the earthy type of sepiolite and palygorskite observed in this study displayed precipitation from fluid enriched in Si, Al, Mg, and minor Fe and depleted in other ions at an earlier stage of offset of the andesitic veins. Continuation of reverse faulting and high shearing stress caused the precipitation of a significant quantity of interlaminated sepiolite. Sepiolite and palygorskite were formed at an earlier stage of fluid interaction relative to smectite in the Tuluanshan Formation.

Key Words—Alteration, Andesite, SEM, TEM, Smectite, Taiwan, Tuluanshan Formation.

INTRODUCTION

Sepiolite and palygorskite occur in a wide range of Earth-surface environments including marine deposits (Bonatti and Joensuu, 1968; Lopez-Aquayo and Lopez-Gonzalez, 1995; Jamoussi *et al.*, 2003; Garcia-Romero *et al.*, 2007), continental sediments (Kolla *et al.*, 1982; Akbulut and Kadir, 2003; Cuevas *et al.*, 2003; Hong *et al.*, 2007), soils (Singer *et al.*, 1998; Akbulut and Kadir, 2003), and hydrothermally affected rock formations (Stephen, 1954; Kirkman and Wallace, 1994; Torres-Ruiz *et al.*, 1994; Sanchez and Galán, 1995; Singer *et al.*, 1998; Karakaya *et al.*, 2004; Romero *et al.*, 2004; Yalcin and Bozkaya, 2004). The distribution of sepiolite and palygorskite is limited to dry areas, given specific Eh, pH, and dissolved-SiO_2 conditions (Preisinger, 1961; Paquet, 1983; Badraoui *et al.*, 1992; Ducloux *et al.*, 1995; Monger and Lynn, 1996). Evidence from activity diagrams indicates that both sepiolite and palygorskite can form from alkaline solutions, sepiolite having high activities of Si and Mg (Preisinger, 1961; Golden *et al.*, 1985; Chen, 1989). Palygorskite also requires Al and/or Fe (Singer, 2002). Sepiolite and palygorskite may transform into smectite under alkaline conditions (Golden *et al.*, 1985). The formation of palygorskite is favored over that of smectite by an increase in either [Mg^{2+}], pH, or [H_4SiO_4] (Singer, 1989).

Sepiolite and palygorskite formed in andesitic rocks on the eastern Coastal Range of Taiwan due to hydrothermal alteration and surficial weathering (Chen and Tung, 1988; Chen *et al.*, 1988). In the Miocene Tuluanshan Formation, smectite was formed in country rocks during late-stage, low-temperature, hydrothermal activity whereas sepiolite precipitated from fluids enriched in Si, Mg, and Fe, and depleted in other ions at an earlier stage of low-temperature, hydrothermal alteration (Ho, 1988; Chen and Tung, 1988; Arranz *et al.*, 2008)). Mineral assemblages with smectite were derived from porphyritic hornblende andesite under the influence of hydrothermal alkaline solutions (Kao *et al.*, 2003). The formation overlies an andesitic core complex that is presumed to be the source of hydrothermal fluids responsible for the Si- and Mg-rich mineralization in the Tuluanshan Formation. The purpose of this study was to confirm that presumption by characterizing the sepiolite and palygorskite in this Formation with respect to their occurrence and distribution in the Tungho (TH) and Chunjih (CJ) areas, using standard mineralogical methods.

* E-mail address of corresponding author: mkwang@ntu.edu.tw
† Present address: Exploration and Development Research Center, Chinese Petroleum Corporation, Taipei, Taiwan
DOI: 10.1346/CCMN.2009.0570502

MATERIALS AND METHODS

Study area

The lowermost exposed stratigraphic unit overlying the Miocene andesitic igneous core is the Tuluanshan Formation, Taiwan, which consists largely of agglomerate, tuff, and tuffaceous sediments, representing a sedimentary accumulation of pyroclastic debris rather than a direct product of volcanic eruption. A thick agglomerate series is exposed in the Tuluanshan ridge, one of the highest peaks in the eastern Coastal Range (Ho, 1988).

Discontinuous limestone lenses occur at and near the top of the agglomerate series along the eastern flank of the Coastal Range. A recent study of nanofossils shows that the upper portion of the Tuluanshan Formation ranges from the middle to late Miocene period to the Miocene/Pliocene boundary (Chi, 1981).

Convergent tectonic processes in eastern Taiwan account for the occurrence of the Tuluanshan Formation. The coastal and central ranges formed as a result of the collision of the east Philippine Sea plate and the west Eurasian plate (Ho, 1988; Lee *et al.*, 2006). The suture of the plates is now represented by the Longitudinal Valley between Taitung and Hualien counties (Figure 1). This valley has been and is still a locus of earthquakes and tectonic activity in eastern Taiwan (Ho, 1988).

Sampling and sample preparation

Outcrops of sepiolite and palygorskite are found in the Tuluanshan Formation, near the town of Tungho (TH) (Taitung County) and at Chunjih (CJ) (Hualien County, near the town of Yuli) in the eastern Coastal Range (Figure 1a). A geologic map of the Tuluanshan Formation (Figure 1b) shows the location of the sampling sites (Chen, 1989). Palygorskite was found in alternating bands (~20−25 cm wide), 15 m from the northern outcrop of sepiolite.

Field surveys have also found occurrences of sepiolite within the fissure and fracture zones of the Tuluanshan Formation. A reverse fault (oriented 005º/54ºW) is found between the agglomerate and the andesite. The sepiolite veins in the TH area are ~1−2 cm wide, and extend in both the northeast and northwest directions from the fault plane. Some sepiolite veins are sigmoidal in shape and easily turn into powder. Broken materials occur on the reverse fault as lenses of sepiolite and are 10−40 cm wide and 1 m long. Figure 2 shows the lenses of sepiolite and country rocks. Two types of sepiolite veins are observed: (1) lenses of yellowish-brown, blocky sepiolite from the TH area; and (2) dark-brown, earthy sepiolite from the CJ area. The earthy sepiolite showed significant intercalated layers. Samples Sep 19-31 were collected from the TH area and Sep 32-40 from the CJ area.

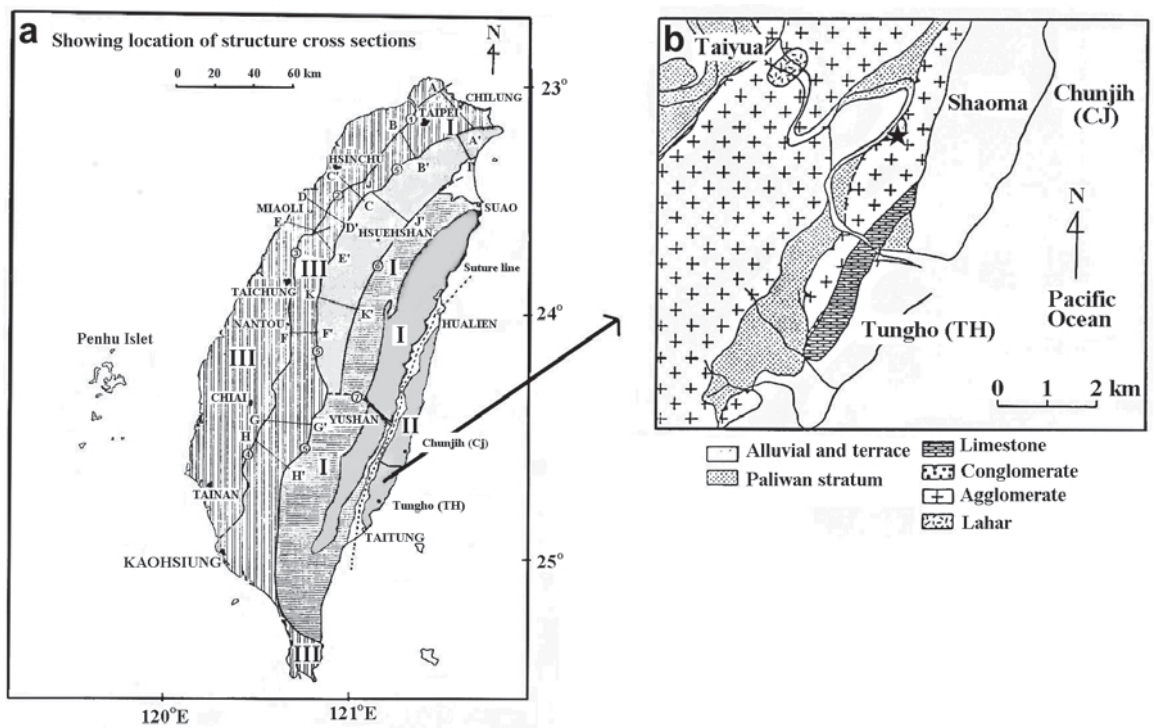

Figure 1. (a) Geologic provinces of Taiwan, (I) central range province, (II) coastal range province, and (III) western foothill province; (b) geologic map of the Tungho and Chunjih areas. ★ denotes the position of the sepiolite lense. The dashed line denotes the suture zone.

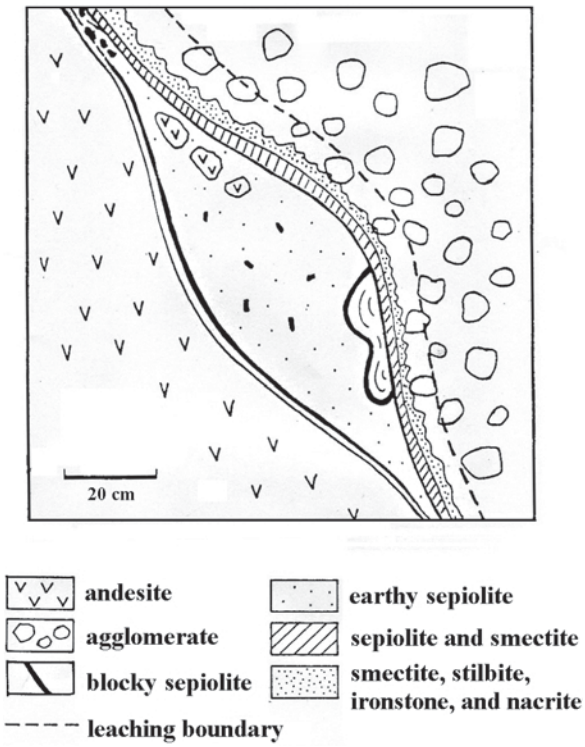

Figure 2. Lenses of sepiolite associated with country rocks (as indicated by ★ in Figure 1b).

Palygorskite outcrops can be classified into six subgroups: (1) gray-white andesite without alteration, consisting of quartz, plagioclase, hornblende, hypersthene, and minor montmorillonite; (2) slight alternation of andesite with Fe-Mg minerals and plagioclase; (3) brown bands (2–5 cm thick) of palygorskite with plagioclase, quartz, hornblende, and smectite; (4) green-gray bands ~1 cm wide, with plagioclase, quartz, hornblende, and smectite; (5) yellow-brown bands ~5–8 cm wide with quartz, plagioclase, and hypersthene; and (6) palygorskite without any alternation of andesite. Boundaries between subgroups 3 and 4 as well as between 4 and 5 were unclear. The palygorskite samples collected from brown bands in subgroup 3 were designated as Pal 14, Pal 26, Pal 30, and Pal 57-60 from the TH area.

Analytical methods

Sixty clay samples from various outcrops of the TH and CJ areas were investigated and dispersed by ultrasonic vibration in deionized water, and the <10 μm particle size-fraction was removed by repeated settling in water. Impurities were largely eliminated from most of the samples by this procedure. The samples were then freeze-dried.

Powder XRD studies were performed using a Rigaku Geiger-flex with Ni-filtered CuKα radiation at 35 kV and 15 mA. Randomly oriented powders of <10 μm particle size-fractions were scanned from 3–65º2θ at 0.02º2θ min^{-1}. The Mg-saturated clays were examined at 25ºC before and after ethylene glycol solvation in order to check for expandable smectite (Jackson, 1979; Pai *et al.*, 1999). The goniometer was calibrated against quartz, and the peaks yielded sufficient intensity to differentiate sepiolite and palygorskite (attapulgite). Sepiolites SepNev-1 (Two Crows, Nevada, USA) and SepSp-1 (Valdemoro, Spain), attapulgite PFL-1 (Gadsden County, Florida, USA), and palygorskite UKP (Warren Quarry, Enderby, Leicestershire, UK) were also analyzed. These reference minerals were supplied by 'Minerals Unlimited' (Ridgecrest, California, USA) and The Clay Minerals Society Source Clays Repository (based at Purdue University, West Lafayette, Indiana, USA).

Differential thermal (DTA) and thermal gravimetric (TG) analyses were performed using a Shimadzu DT-30 thermal analyzer and a Netzsch STA 409 thermal gravimeter, respectively, and the system was heated at ~10ºC/min. Infrared analyses were conducted on freeze-dried portions of clays using a Biorad model FTS-7 Fourier Transform Infrared Spectrometer. Infrared samples were prepared by pressing dried clay samples into KBr discs (weight ratio of clay:KBr = 0.5:300 mg).

Petrographic microscopy, SEM, and TEM were used to examine particle morphology. Clays and argillized rocks were also examined using a polarizing petrographic microscope to determine textural and optical properties. Samples examined included epoxy-impregnated thin sections and powdered samples on a glass slide, which were viewed in water or in an immersion liquid. Ground samples were examined using an Hitachi-520 SEM to view the morphology and perform elemental analyses of sepiolite and palygorskite. A single drop of clay suspension was allowed to dry on a copper grid (300 mesh, 3.05 mm in diameter) coated with a carbon film before examining it using an Hitachi HU 600 transmission electron microscope operated at 75 kV. The chemical compositions of sepiolite and palygorskite were established using the ARL-SEMQ electron microprobe (Central Geological Survey, Taiwan), at an accelerating voltage of 15 kV, a sample current of 1.5 μA, and counting twice with a 20 s interval. The defocus of the electron beam was 5 to 6 μm.

RESULTS AND INTERPRETATION

Identification of minerals

XRD of Sep 26 and Pal 30 as examples. X-ray diffraction data results (Table 1) revealed a strong XRD reflection at 1.19 nm for sample Sep 26, with moderate reflections at 0.449, 0.429, 0.373, 0.330, 0.316, 0.2607, 0.2580, and 0.2557 nm. Reflections similar to these were also observed in samples SepNev-1 and SepSp-1, which compared well with JCPDS 13-595 (Table 1). For palygorskite (Pal 30), an intense XRD peak occurred at

Table 1. *d* spacings (nm) of sepiolites, Sep 26, SpeNev-1, SepSp-1, and JCPDS-13-595.

TH (Sep 26)		Nevada (SepNev-1)		Spain (SepSp-1)			
$d_{(obs)}$ (nm)	I/I_o	$d_{(obs)}$ (nm)	I/I_o	$d_{(obs)}$ (nm)	I/I_o	JCPDS *d* values	13-595 I/I_o
1.19	100	1.2	100	1.2	100	12.1	100
0.741	4	0.747	3	0.744	3	7.47	10
0.656	3	0.661	6	0.660	4	6.73	6
0.499	3	0.501	3	0.501	4	5.01	8
0.472	<1	–	–	–	–	–	–
0.449	11	0.452	13	0.450	13	4.5	25
0.429	20	0.430	23	0.430	26	4.31	40
0.402	1	0.404	6	0.400	2	4.02	8
0.393	1	–	–	–	–	–	–
0.373	15	0.375	14	0.374	13	3.75	30
0.351	3	0.343	13	0.353	3	3.53	12
–	–	0.336	9	–	–	–	–
0.33	22	0.334	30	0.332	17	3.37	30
–	–	0.329	15	–	–	–	–
0.316	13	0.321	16	0.318	14	3.2	35
0.303	3	0.302	2	0.304	3	3.05	12
–	–	–	–	–	–	2.932	4
0.2814	1	–	–	–	–	2.825	8
–	–	–	–	–	–	2.771	4
0.2660	4	0.2674	5	0.2679	6	2.691	20
0.2607	10	0.2618	10	0.2618	11	2.617	30
0.2580	12	0.2585	15	0.2582	14	2.586	8
0.2557	18	0.2557	19	0.2557	20	2.56	55
–	–	0.2455	4	–	–	2.479	6
–	–	0.2442	8	0.2439	7	2.449	25
0.2430	8	0.2430	7	–	–	–	–
0.2387	4	0.2392	2	0.2392	5	2.406	16
0.2252	8	0.2259	9	0.2256	9	2.263	30
0.2202	2	–	–	–	–	2.206	4
0.2113	2	0.2129	2	–	–	2.125	8
0.2051	4	0.2056	3	0.2060	3	2.069	20

1.05 nm, with moderate reflections at 0.638, 0.534, 0.446, 0.314, 0.293, 0.2522, 0.2227, and 0.2113 nm. XRD reflections of palygorskite reference materials UKP and PFL-1 were similar to those of sample Pal 30 (Table 2). However, the powder XRD patterns of Pal 30 contain quartz, feldspar, and montmorillonite. The 1.47 nm reflection expanded to 1.74 nm when the Mg-saturated sample was solvated with ethylene glycol at 25ºC (Chen, 1989).

The position of the d_{110} reflection remained unchanged while the 1.19 nm reflection increased in intensity. The Sep 26 sample heated at 450ºC showed diffuse XRD reflections and the *d* values were 1.187, 1.011, 0.807, 0.439, 0.434, 0.313, and 0.255 nm, while the 0.439 nm reflection gained in intensity. The sample is interpreted as a dehydrated sepiolite (Preisinger, 1961). The XRD patterns of Sep 26 heated at 530, 600, and 730ºC were similar to those of Sep 26 heated at 450ºC. The d_{020}, d_{110}, d_{120}, and d_{061} peaks decreased in intensity. The powder XRD patterns of earthy sepiolite from country rocks of the CJ area contained quartz in many cases.

Thermal analyses

Sepiolite (Sep 26) displayed four broad endothermic reactions at 113, 232, 372, and 818ºC (Figure 3a). The DTA pattern of reference sample SepSp-1, which is similar to that of Sep 26, consists of three endothermic reactions associated with the elimination of hydrated water and of an intense exothermic peak near 840ºC (Sep 26) and 858ºC (Sep Sp-1). Thermogravimetric analysis (TGA) of Sep 26 under normal heating at 850ºC exhibits a progressive weight loss of 21%. Heating at 170ºC resulted in loss of ~12.8 wt.% of hydrated and channel water, and heating at 175−470ºC caused loss of ~5.5 wt.% of structural water.

Palygorskite (Pal 30) exhibited distinct endothermic peaks at 90º and 123ºC, broad endothermic peaks at 235º, 452º, and 552ºC, and an exothermic peak at 865ºC (Figure 3b). Thermogravimetric analysis of Pal 30 showed that heating at 850ºC caused a progressive weight loss of 18.3 wt.% H_2O. Heating at 180ºC released ~10.6 wt.% of hydrated and channel water, and heating at 180−520ºC released ~6.3 wt.% of structural water (Chen, 1989). The thermal behavior of Pal 30 is quite similar to that of

Table 2. *d* spacings of palygorskites, UKP, PEL-1, and Pal 30.

UKP		PFL-1			Pal 30		
$d_{(obs)}$ (nm)	I/I_o	$d_{(obs)}$ (nm)		I/I_o	$d_{(obs)}$ (nm)	I/I_o	*hkl*
1.03	100	1.05		100	1.05	100	110
0.633	25	0.642		13	0.638	33	200
0.611	1	–		–	0.616	23	210
0.539	11	0.537		13	0.534	25	130
0.447	22	0.446		35	0.446	66	40
–	–	0.445		13	–	–	21
–	–	0.426*		44	–	–	–
0.426	4	0.423		30	0.421	66	$\bar{1}21$
0.413	3	0.413	B	14	0.419	49	121
0.407	5	–		–	0.403[a]	66	$\bar{2}01$
0.388	1	0.388	B	7	0.388[a]	30	031,211
–	–	–		–	0.374[a]	54	$\bar{1}31$
–	–	0.368	B	11	0.367	39	$\bar{2}21$
0.365	7	–		–	0.364	56	240
0.344	2	0.345	B	9	0.346	39	330
0.334	2	0.344*		93	–	–	$\bar{2}31,\bar{3}01$
0.327	4	–		–	–	–	$\bar{1}41$
0.323	5	0.323		33	–	–	141
0.317	30	0.317	B	30	–	–	400
–	–	–		–	0.314	70	410
0.308	5	0.308		11	0.308 B	49	340
–	–	–		–	0.300b	30	420
–	–	–		–	0.293	33	51
0.288	1	–		–	0.29	23	160
–	–	–		–	0.2837	16	$\bar{1}51$
–	–	0.2788		9	0.2797	13	430
–	–	0.2687		9	0.2691	16	260
0.2675	2	–		–	0.2652	31	$\bar{3}41$
0.2607	4	0.2607		20	– B	–	341
0.2583	11	0.2582		20	0.2606	43	440
–	–	–		–	0.2564[b]	69	2
0.2536	7	0.2539		27	0.2535[b]	82	$\bar{1}61$
0.2515	3	0.2515		27	0.2522	82	161
0.2506	3	–		–	–	–	$\bar{1}12$
–	–	–		–	0.2455[c]	28	431
–	–	–		–	0.2381	20	261
0.233	1	–		–	–	–	530
–	–	0.2279		7	0.2280[c]	23	71
0.2233B	1	0.2233		7	0.2227	23	80
0.2151B	2	0.2151	B	8	0.2151 B	16	$\bar{5}31$
0.211	7	0.2117		10	0.2113	23	$\bar{2}42$
					0.1978	8	412,$\bar{6}01$
					0.1817	25	$\bar{5}12$
					0.1795	13	641,$\bar{1}72$
					0.1774	11	291
					0.1738	8	452
					0.1713[b]	8	701
					0.1664	11	$\bar{2}03$
					0.154	20	680
					0.1528	15	$\bar{8}11,\bar{2}92$

B: broad XRD peak
*: quartz
a: overlap with plagioclase
b: overlap with montmorillonite
c: overlap with quartz

reference samples UKP and PFL-1 (Figure 3b). The thermal analyses of Sep 26 and Pal 30 are similar to those of samples reported by Singer (1989, 2002).

Infrared analysis

Infrared spectra of sepiolite and palygorskite (Figure 4a,b) are clearly very much affected by the hydration state of the minerals. The IR spectrum of Sep 26 shows absorption bands at 3700, 3625, 3575, 3430, 3280, 1665, 1640, 1215, 1205, 1083, 1040, 1010, 1000, 790, 770, 690, 650, 530, 490, 475, and 450 cm^{-1}. The 3700 cm^{-1} absorption band of Sep 26 shifts to 3720 cm^{-1} under vacuum as adsorbed surface water is removed and is attributed to the stretching vibrations of structural SiO-H (silanol groups) at the edges of the tetrahedral sheets (Ahlrichs *et al.*, 1975; Serna *et al.*, 1977). The 3680 cm^{-1} IR stretching vibration arises from the $(Mg)_3OH$ in the octahedral sheet (Serratosa, 1978). Bands at 3575 and 1640 cm^{-1} occur due to the OH-stretching bands of coordinated H_2O. These bands are also affected by dehydration. The IR band near 1200 cm^{-1} is attributed to Si-O-Si bending vibration. On the other hand, the 690 and 646 cm^{-1} absorption bands represent a deformation of OH in the trioctahedral 2:1 layer silicate. The IR spectrum of palygorskite displays 3620, 3595, 3555, 3450, 3280, 1645, 1190, 1125, 1100, 1035, 995, 950, 915, 645, 585, 520, 495, and 450 cm^{-1} absorption bands. A 3700–3500 cm^{-1} broad absorption band is attributed to the stretching vibrations of structural OH coordinated to octahedral Al. As coordinated H_2O is lost with heating, absorption bands from structural OH stretching modes are revealed at 3657 and 3644 cm^{-1} (Hayashi *et al.*, 1969; Van Scoyoc *et al.*, 1979). Additional absorption bands of coordinated H_2O can be observed at 1645 cm^{-1}. All these absorption bands are affected by hydration-dehydration at low temperatures. Small absorption bands at 1190, 1125, 1100, 1035, and 995 cm^{-1} are due to Si-O stretching. Infrared absorption bands of palygorskite between 1190 and 1125 cm^{-1} are assigned to Si-O-Si groups, which serve as bridges between two alternating alumino-Mg-silicate ribbons (Yariv, 1986; Singer, 1989, 2002).

Petrographic microscopy, SEM, TEM

Petrography of Sep 34 showed irregular, compacted sepiolite associated with opaque minerals under crossed

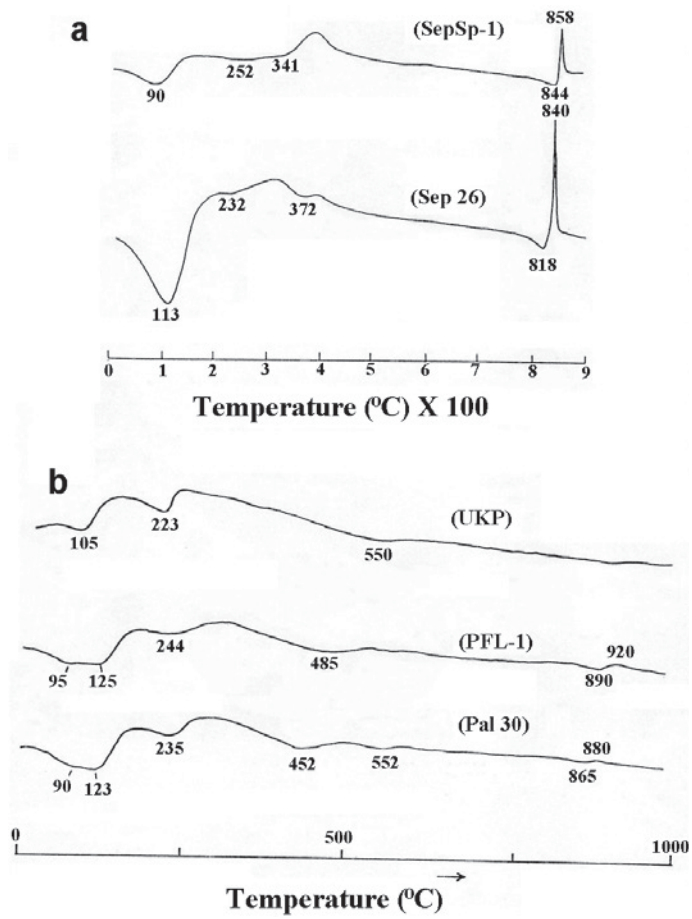

Figure 3. (a) DTA traces of samples SepSp-1 and Sep 26; (b) DTA traces of samples UKP, PFL-1, and Pal 30 of palygorskite.

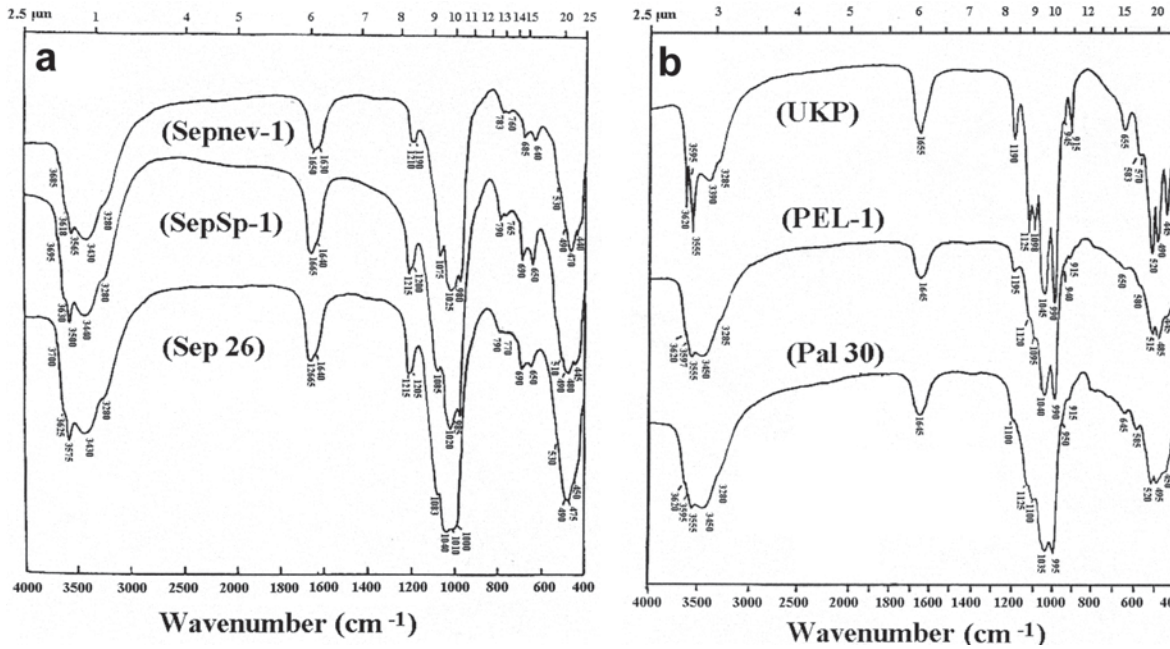

Figure 4. IR spectra of (a) sepiolite – SepNev-1, SepSp-1 and Sep 26 from the TH area; and (b) of palygorskite – UKP, PFL-1 and Pal 30.

nicols (Figure 5a). Both sepiolite and palygorskite were easily identified by TEM on the basis of their fibrous morphology. Sep 26 was present as fibrous sepiolite (Figure 5b). However, Sep 34 showed random orientation of the fibrous morphology (Figure 5c). Palygorskite fibers are usually intimately mixed with other mineral

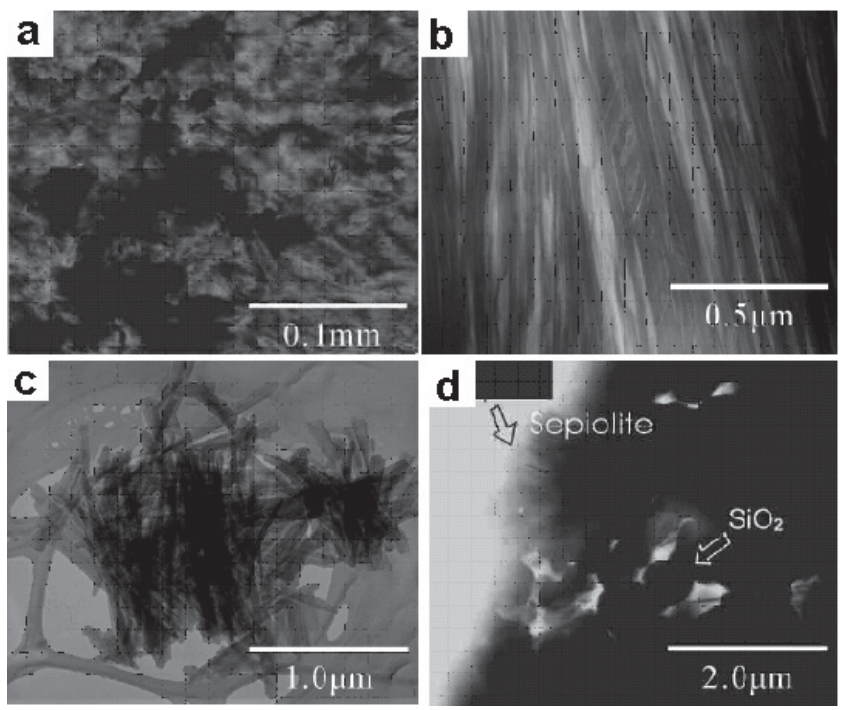

Figure 5. (a) Photomicrograph of earthy sepiolite from the CJ area (Sep 34) showing irregular, compacted sepiolite associated with opaque minerals under cross-polarized light. TEM images of blocky sepiolite (Sep 26 from TH area) (b), earthy sepiolite (Sep 34 from the CJ area) (c), and palygorskite (Pal 30) (d).

components, commonly smectite, feldspar, and quartz. The palygorskite fibers appear to be aggregated into bundles or sheaves. The length and width of palygorskite associated with quartz are from 0.2−1.5 μm and 0.01−0.03 μm, respectively (Figure 5d). Distinguishing between sepiolite and palygorskite is difficult; however, sepiolite seems to demonstrate a greater width to thickness ratio than palygorskite and tends to fray more at the end of the bundle (Vivaldi and Robertson, 1971; Singer, 1989, 2002).

Scanning electron micrographs of sepiolite showed that it had oriented fibers. Either blocky or earthy-type sepiolite is present in the intercalated layers (Figure 6a,b). Two sets of intercalated sepiolite layers demonstrated right angles of extension direction (Figure 6c). An SEM image of fibrous palygorskite associated with montmorillonite showed the dissolution of the palygorskite surfaces (Figure 6d). The pore-bridging fibrous palygorskite is closely associated with montmorillonite (Figure 6e). Some montmorillonite particles were partially fibrous under high-resolution TEM (Chen, 1989).

Chemical compositions

Earthy sepiolite contained large amounts of Si due to contamination with other minerals (*e.g.* SiO_2). The composition of palygorskite varies significantly and is comparable to that of smectite. Isomorphous substitution of Al for Si in the tetrahedral site is very limited. Occupancy in the tetrahedral sites of palygorskite ranges from $(Si_{7.88}Al_{0.12})$ to $(Si_{7.34}Al_{0.66})$ (Singer, 2002). Newman and Brown (1987) classified this clay as a dioctahedral palygorskite. Li *et al*. (2007) reported Fe-rich palygorskite formed in eastern China. The chemical composition of palygorskite (Pal 30) showed high Si, Mg, and Al contents, which may be created by the minor plagioclase, quartz, and montmorillonite contents in the Pal 30 sample.

DISCUSSION

Stability diagrams indicate that alkaline solutions and high activities of Si and Mg are needed to form palygorskite and sepiolite (Golden *et al.*, 1985). Singer

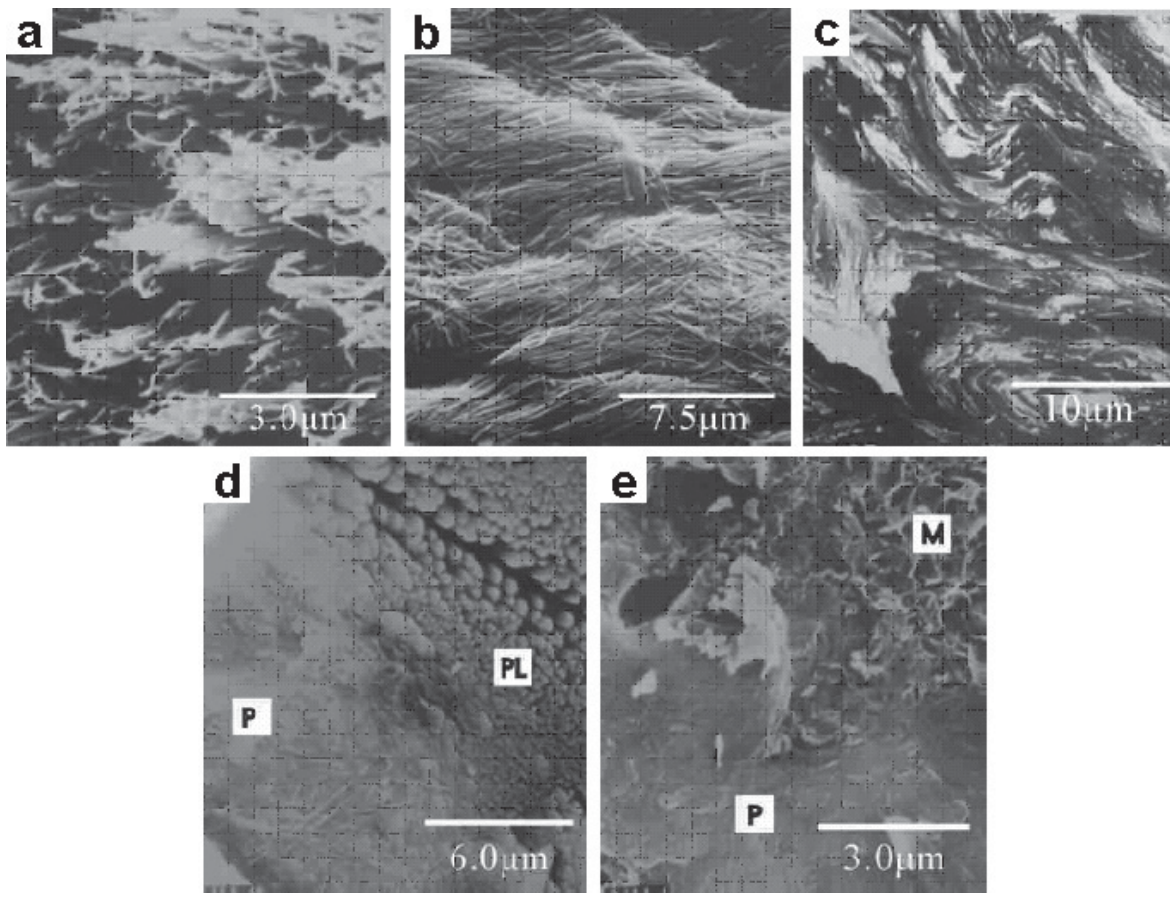

Figure 6. SEM images of (a) blocky sepiolite, and (b) earthy sepiolite showing shearing stress; (c) two sets of intercalated sepiolite layers and palygorskite, (d) palygorskite (P) associated with plagioclase (PL), and (e) palygorskite (P) associated with montmorillonite (M).

(2002) reported that acid-dissolution data for the two Australian palygorskites indicated that both Fe and Mg are preferentially dissolved over Al, suggesting that the small amounts of Al ions are concentrated in the more interior positions, while the large Mg and Fe ions are situated in edge positions. The sepiolite stability diagram indicates that Mg activities have to be even greater. Certain thresholds of pH, Si, and Mg concentrations have been demonstrated where palygorskite was stable (Singer and Norrish, 1974). Similar physical and chemical thermal microenvironments related to pore space may also be required. Interstitial solutions in contact with altering basement rocks may actually be supersaturated with respect to both sepiolite and palygorskite, particularly when some hydrothermal activity is invoked (Bonatti *et al.*, 1983; Birsoy, 2002).

Sepiolite and palygorskite occur alone or with chalcedony in veins of the Tuluanshan Formation. The hydrothermal solutions provided high concentrations of Si and Mg. These hydrothermal solutions penetrated into the andesite or andesitic agglomerate region and caused the dissolution of Fe and Mg from hornblende and pyroxene. With appropriate Si, Mg, Al, and Fe concentrations and pH in the hydrothermal solutions, precipitation of sepiolite and palygorskite is possible (Birsoy, 2002). The reverse fault of andesite was located near the andesitic agglomerate and formed a local offset. Thus, large concentrations of Si and Mg filled this reverse fault and sepiolite precipitated in these fractures. The pH of alkaline solutions (*i.e.* hydrothermal solution) in the TH and CJ areas was between 8.0 and 9.0 (Chen, 1989).

Along the continuation of the reverse fault sites, a significant amount of intercalated sepiolite was formed. Two sets of intercalated sepiolite layers may indicate two offsets. XRD analysis and TEM and SEM investigations clearly show that palygorskite precipitated onto the surface of plagioclase, showing local dissolution of plagioclase under appropriate micro-environmental conditions. Hydrothermal solutions penetrating into andesite rocks caused the dissolution of Si and Mg. Transmission electron microscopy of palygorskite showed no intercalated layers, indicating the lack of influence of any shear stress or reverse faulting. Smectitization of country rocks may occur at the stage of low-*T* hydrothermal alteration in the Tuluanshan Formation.

CONCLUSIONS

The origin of the Longitudinal Valley (a fault) has been recognized for a long time. Active faulting is indicated by high seismicity, many large earthquakes through history, and fault scarps that cut alluvial deposits on the valley floor. The Longitudinal Valley is a ramp valley in accordance with the hypothesis that each side of the valley is bounded by a high-angle upthrust. The existence of the Central Range fault along the western margin of the Longitudinal Valley is still a subject of debate, however. Further investigation is needed to study this tectonic problem, the hydrothermal alteration, and the formation of sepiolite and palygorskite from the Tuluanshan Formation, Eastern Taiwan

ACKNOWLEDGMENTS

This study was supported by the National Science Council, Taiwan, under projects NSC 88-2116-M-047-002, 89-2621-B-002-006 and 89-2621-B002-019.

REFERENCES

Ahlrichs, J.L., Serna, C., and Serratosa, J.M. (1975) Structural hydroxyls in sepiolite. *Clays and Clay Minerals*, **23**, 119–124.

Akbulut, A. and Kadir, S. (2003) The geology and origin of sepiolite, palygorskite and saponite in Neogene lacustrine sediments of the Serinhisar-Acipayam Basin, SW Turkey. *Clays and Clay Minerals*, **51**, 279–292.

Arranz, E., Lago, M., Bastida, J., Galé, C, Soriano, J., and Ubide, T. (2008) Hydrothermal macroscopic Fe-sepiolite from Oujda Mounts (Middle Atlas, Eastern Morocco). *Journal of African Earth Sciences*, **52**, 81–88.

Badraoui, M., Bloom, P.R., and Bouabid, R. (1992) Palygorskite-smectite association in Xerochrepts of the High Chaouia Region of Morocco. *Soil Science Society of America Journal*, **56**, 1640–1646.

Birsoy, R. (2002) Formation of sepiolite–palygorskite and related minerals from solution. *Clays and Clay Minerals*, **50**, 736–345.

Bonatti, E. and Joensuu, O. (1968) Palygorskite from Altantic deep sea sediments. *American Mineralogist*, **53**, 975–983.

Bonatti, E., Simmons, E.C., Berger, D., Hamlyn, P.R., and Lawrence, J. (1983) Ultramafic rock–seawater interaction in the oceanic crust: Mg-silicate (sepiolite) deposit from Indian floor. *Earth and Planetary Science Letters*, **62**, 229–238.

Chen, R.C. (1989) Mineralogical Study on the Sepiolite and Palygorskite from Tungho, Coastal Range of Taiwan. Master Thesis, National Taiwan University, Taipei, Taiwan. 108 pp.

Chen, R.C. and Tung, S.K. (1988) *An occurrence of sepiolite from Tungho coastal range, eastern Taiwan and its tectonic implication.* Symposium on Arc-Continent Collision and Orogenic Sedimentation in Eastern Taiwan and Ancient Analogs. Princeton University, New Jersey, USA, 26 pp.

Chen, R.C., Yao, T.M., and Tien, P.L. (1988) Sepiolite from Tungho, coastal range, eastern Taiwan. *Geological Society of China. Annual Meeting Program with Abstract*, 57 pp.

Chi, W.R. (1981) Calcareous nannoplankton biostratigraph and stratigraphic correlation of the Mesozoic and Cenozoic sequences in central, southern and eastern Taiwan. *10th Convention, Indonesian Petroleum Association*, pp. 3–49.

Cuevas, De La Villa, R.V., Ramirez, S., Petit, S., Meunier, A., and Leguey, S. (2003) Chemistry of Mg smectites in lacustrine sediments from the Vicalvatro sepiolite deposit, Madrid Neogene Basin (Spain). *Clays and Clay Minerals*, **51**, 457–472.

Ducloux, J., Delhoume, J.P., Petit, S., and Decarreau, A. (1995) Clay differentiation in Aridisols of northern Mexico. *Soil Science Society of America Journal*, **59**, 269–276.

Garcia-Romero, E., Suarez, M., Santarten, J., and Alvarez, A. (2007) Crystallochemical characterization of palygorskite and sepiolite from the Allou Kagne deposit, Senegal. *Clays and Clay Minerals*, **55**, 606–617.

Golden, D.C., Dixon, J.B., Shadfan, H., and Kippenberger,

L.A. (1985) Palygorskite and sepiolite alteration to smectite under alkaline conditions. *Clays and Clay Minerals*, **33**, 44–50.

Hayashi, H., Otsuka, R., and Imai, N. (1969) Infrared study of sepiolite and palygorskite on heating. *America Mineralogist*, **54**, 1613–1624.

Ho, C.S. (1988) *An Introduction to the Geology of Taiwan-Explanatory Text of the Geologic Map of Taiwan*, 2nd edition. Published by Central Geological Survey, The Ministry of Economic Affairs, Taipei, Taiwan, 192 pp.

Hong, H.L., Yu, N., Xiao, P., Zhu, Y.H., Zhang, K.X., and Xiang, S.Y. (2007) Authigenic palygorskite in Miocene sediments in Linxia basin, Gansu, northwestern China. *Clay Minerals*, **42**, 45–58.

Jackson, M.L. (1979) *Soil Chemical Analysis*, *Advanced Course*, 2nd edition. University of Wisconsin, Madison, USA. 497 pp.

Jamoussi, F., Aboud, A.B., and Lopez-Galindo, A. (2003) Palygorskite genesis through silicate transformation in Tunisian continental Eocene deposits. *Clay Minerals*, **35**, 433–441.

Kao, N.C., Wang, M.K., Chiang, P.N., and Chang, S.S. (2003) Characterization of wheat-rice-stone developed from porphyritic hornblende andesite. *Applied Clay Science*, **23**, 337–346.

Karakaya, N., Karakaya, M.C., Temel, A., and Kupeli, C.E. (2004) Mineralogical and chemical characterization of sepiolite occurrences at Karapinar (Konya Basin, Turkey). *Clays and Clay Minerals*, **52**, 495–509.

Kirkman, J.H. and Wallace, R.C. (1994) Palygorskite in the regolith from the Mocan desert, North Island, New Zealand. *Clay Minerals*, **29**, 265–272.

Kolla, V., Kostecki, J., and Robinson, F. (1982) Distributions and origins of clay minerals and quartz in surface sediments of the Arabian Sea. *Journal of Sedimentary Petrology*, **51,** 563–569.

Lee, J.C., Chu, H.T., Angellier, J., Hu, J.C., Chen, H.Y., and Yu, S.B. (2006) Quantitative analysis of surface coseismic faulting and post-seismic creep accompanying the 2003, *Mw* = 6.5, Chengkung eqrthquake in eastern Taiwan. *Journal of Geophysical Research*, **111,** B02405.

Li, Z., He, K., Yin, L., Xiong, F., and Zheng, Y.C. (2007) Crystallochemistry of Fe-rich palygorskite from eastern China. *Clay Minerals*, **42**, 453–461.

Lopez-Aguayo, F. and Lopez-Gonzalez, J.M. (1995) Fibrous clays in the Almazan Basin (Iberian Range, Spain): Genetic pattern in calcareous lacustrine environment. *Clay Minerals*, **30**, 395–406.

Monger, H.C. and Lynn, W.C. (1996) Clay mineralogy at the desert project and the Rincon surface study area. Pp. 113–155 in: *Supplement to the Desert Project Soil Monograph* (L.H. Gile and R.J. Ahrens, editors). Vol. II. National Soil Survey Center, Lincoln, Nebraska, USA.

Newman, A.C. and Brown, G. (1987) The chemical constitution of clays. Pp. 1–128 in: *Chemistry of Clays and Clay Minerals* (A.C.D. Newman, editor). Monograph **6**, Mineralogical Society, London.

Pai, C.W., Wang, M.K., Wang, W.M., and Houng, K.H. (1999) Smectites in iron-rich calcareous soil and black soils of Taiwan. *Clays and Clay Minerals*, **47**, 389–398.

Paquet, H. (1983) Stability, instability and significance of attapulgite in the calcretes of Mediterranean and tropical area with marked dry season. *Sciences Géologiques Mémoires (Strasbourg)*, **72**, 131–140.

Preisinger, A. (1961) Sepiolite and related compounds: its stability and application. Proceedings of the 10th National Conference. *Clays and Clay Minerals*, **11**, 365–371.

Romero, E.G., Barrios, M.S., and Bustillo Revueta, M.A. (2004) Characteristics of Mg-palygorskite in Miocene rocks, Madrid Basin (Spain). *Clays and Clay Minerals*, **52**, 484–494.

Sanchez, C. and Galán, E. (1995) An approach to the genesis of palygorskite in a Neogene-Quaternary continental basin, using principal factor analysis. *Clay Minerals*, **30**, 225–238.

Serna, C., Van Scoyoc, G.E., and Ahlrichs, J.L. (1977) Hydroxyl groups and water in palygorskite. *American Mineralogist*, **62**, 784–792.

Serratosa, J.M. (1978) Surface properties of fibrous clay minerals (palygorskite and sepiolite). Pp. 99–109 in: *Proceedings of the International Clay Conference* (M.M. Mortland and V.C. Farmer, editors). Elsevier Science, Amsterdam.

Singer, A. (1989) Palygorskite and sepiolite group minerals. Pp. 829–872 in: *Minerals in Soil Environments* (J.B. Dixon and S.B. Weed, editors). 2nd edition, SSSA Book Series 1, Soil Science Society of America, Madison, Wisconsin, USA.

Singer, A. (2002) Palygorskite and sepiolite. Pp. 555–583 in: *Soil Mineralogy with Environmental Applications* (J.B. Dixon and D.G. Schulze, editors) SSSA Book Series, **7**, Soil Science Society of America, Madison, Wisconsin, USA.

Singer, A. and Norrish, K. (1974) Pedogenic palygorskite occurrences in Australia. *American Mineralogist*, **59**, 508–517.

Singer, A., Stahr, K., and Zarei, M. (1998) Characteristics and origin of sepiolite (Meerschaum) from Central Somalia. *Clay Minerals*, **33**, 349–361.

Stephen, L. (1954) An occurrence of palygorskite in the Shetland Isles. *Mineralogical Magazine*, **30,** 471–480.

Torres-Ruiz, J., Lopez, A., and Gonzalez-Lopez, J.M. (1994) Geochemistry of Spanish sepiolite-plygorskite deposits: Genetic considerations based on trace elements and isotopes. *Chemical Geology*, **112**, 221–245.

Van Scoyoc, G.E., Serna, C.J., and Ahlrichs, J.L. (1979) Structural changes in palygorskite during dehydration and dehydroxylation. *America Mineralogist*, **64**, 215–223.

Vivaldi, M.J.L. and Robertson, R.H. (1971) Palygorskite and sepiolite (the hormites). Pp. 255–275 in: *The Electron-Optical Investigation of Clays* (J.A. Gard, editor). Mineralogical Society, London.

Yalcin, H. and Bozkaya, O. (2004) Ultramafic-rock-hosted vein sepiolite occurrences in the Ankara Ophiolitic Melange, Central Anatolia, Turkey. *Clays and Clay Minerals*, **52**, 227–239.

Yariv, S. (1986) Infrared evidence for the occurrence of SiO groups with double-bond character in antigorite, sepiolite and palygorskite. *Clay Minerals*, **21**, 925–936.

(*Received 26 March 2008; revised 16 March 2009; Ms. 0147; A.E. M.A. Velbel*)